LBL-10884

To be presented at the 5th SPE International Symposium
on Oilfield and Geothermal Chemistry, Stanford, CA,
May 28-30, 1980

DIVALENT ION EXCHANGE WITH ALKALI

A. L. Bunge, G. Klein, and C. J. Radke

May 1980

Prepared for the U.S. Department of Energy
under Contract W-7405-ENG-48

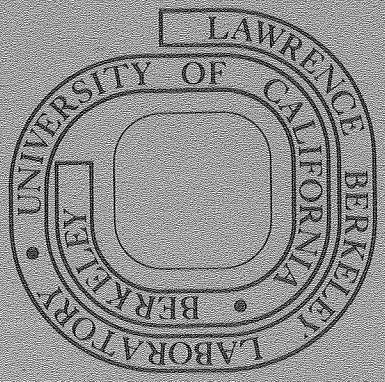

SPE 8995

SPE
Society of Petroleum Engineers of AIME

DIVALENT ION EXCHANGE WITH ALKALI

by A. L. Bunge, G. Klein, and C. J. Radke, U. of California

This paper was presented at the SPE Fifth International Symposium on Oilfield and Geothermal Chemistry, held in Stanford, California, May 28-30, 1980. The material is subject to correction by the author. Permission to copy is restricted to an abstract of not more than 300 words. Write: 6200 N. Central Expwy., Dallas, Texas 75206.

ABSTRACT

Exchange of hardness ions is important in enhanced oil recovery with chemical additives. In both micellar-polymer and caustic flooding processes, multivalent ions released from rock surfaces can interact with anionic surfactants, rendering them preferentially oil soluble and/or insoluble in water. Because hardness cations are sparingly soluble and precipitate in alkaline solutions, such solutions may be more efficient as surfactant flood preflushes than are softened brines. Multivalent ion precipitation may also occur in alkaline waterflooding. To permit design of such processes, this paper presents a chromatographic theory for simultaneous ion exchange with precipitation of divalent ions.

Theoretical effluent histories and concentration profiles are presented for the cases of finite pulses and continuous injection of hydroxide ions into linear cores. Complete capture of the insoluble salt particles is assumed. Results are given for the case of instantaneous equilibration of the solution with the precipitate, as well for the case of complete nonequilibrium, in which the solid precipitate does not redissolve.

The efficiency of alkaline preflushing is shown to depend on the exchange isotherm, initial divalent loading of the rock, injected pH and salinity, the solubility product of the precipitated salt, and pulse size. The effect of slug size on complete equilibrium removal of hardness ions is reduced efficiency with increasing size until a critical volume approximating continuous injection is reached. Increasing injected pH and salinity provides a more favorable response. Experimental data for Berea sandstone and an argillaceous sand compare favorably with the proposed theory.

References and illustrations at end of paper.

INTRODUCTION

The presence of multivalent cations in reservoir brines can profoundly affect the oil recovery efficiency of micellar or polymer slugs. These chemicals can react with hardness cations present to produce water insoluble constituents. Removal of divalent cations, such as magnesium or calcium, with softened brines has been studied extensively (1-7). Problems with reservoir heterogeneities, and concomitant incomplete sweep, are legion. Equally important, however, is the strong preference of most reservoir rock for calcium, which means the large volumes of preflush are required even in the swept zones to obtain the desired low concentrations of hardness ions (2,3,7,8).

Campbell (8), and Holm and Robertson (9) have proposed using chemicals such as sodium hydroxide or sodium orthosilicate in a preflush to react with multivalent cations by precipitation. Currently, a field test of this idea is underway (10).

Alkaline waterflooding of reservoirs containing acidic crude oils has been studied by several workers (11-14) including several field tests (15-18). The naturally occurring acids react with strong base to produce anionic surface active agents, which may improve oil recovery (13,19). In the alkaline flooding process, precipitation of hardness ions will occur unless extensive soft brine preflushing is effected (19). Such precipitation will delay hydroxide transport and reduce oil recovery efficiency.

To date alkaline processes involving in-situ precipitation have been tackled only experimentally by column studies of multivalent cation removal (8) or of oil displacement (9). No current theory exists to permit rational understanding and design. This paper presents a linear chromatographic theory to predict quantitatively hydroxide and divalent cation

concentration profiles and effluent histories. The model is an extension of previous work on ion exchange with precipitation (20-23) to oil recovery systems. The important application of a finite pulse, however, is formulated for the first time. In the theoretical framework only a single hardness species, such as calcium, is considered, and only precipitation of the hydroxide salt is permitted. Before outlining the theory, we briefly review the ion-exchange and precipitation chemistry of divalent ions.

DIVALENT ION CHEMISTRY

Ion Exchange

Various relations have been proposed for describing sodium-calcium distribution between the reservoir rock and the aqueous solution (24). We employ the mass-action approach in which exchange sites, M, are considered to be separate chemical species:

$$2Na^{+} + M_2Ca \rightleftharpoons 2MNa + Ca^{++} \qquad (1)$$

Replacement of the bivalent calcium ion with two monovalent sodium ions preserves electroneutrality of the solid surface. An equilibrium ion-exchange constant, K_I, is defined for reaction (1) as

$$K_I \equiv \frac{q_{Na}^2 C_{Ca}}{q_{Ca} C_{Na}^2} , \qquad (2)$$

where C and q are the ion concentrations in equivalents per unit volume of solution and per unit mass of solid, respectively. The solution salinity is the combined sodium and calcium equivalent concentrations,

$$C_s = C_{Na} + C_{Ca} , \qquad (3)$$

and, likewise, the total cation exchange capacity, Q, is the sum of the species solid concentrations in equivalents per unit mass of solid:

$$Q = q_{Na} + q_{Ca} . \qquad (4)$$

Equations (3) and (4) are essentially statements of electroneutrality in the solution and surface phases. It is convenient to define equivalent fractions of calcium ions in each phase by dividing the calcium concentration by the total cation concentration of each phase:

$$x \equiv \frac{C_{Ca}}{C_s} , \qquad (5a)$$

and

$$y \equiv \frac{q_{Ca}}{Q} . \qquad (5b)$$

When expressed in equivalent fractions, the equilibrium relation in Eqn. (2) defines a new dimensionless ion-exchange equilibrium constant, β :

$$\beta \equiv \frac{K_I C_s}{Q} = \frac{(1-y)^2}{y} \frac{x}{(1-x)^2} . \qquad (6)$$

Notice that computation of the equivalent fraction of calcium associated with the solid, y, requires both the solute equivalent fraction, x, and the total solution salinity. In this study, we do not consider changes in the exchange reaction (1) with changes in the solution pH. As the hydroxyl concentration in solution rises, additional anionic exchange sites may be exposed due to surface hydrolysis. Such additional exchange capacity is not accounted for; hence, this theory is a first approximation.

Ion Precipitation

Precipitation of the slightly soluble salt, calcium hydroxide, obeys the following reaction,

$$Ca(OH)_2(s) \rightleftharpoons Ca^{++} + 2OH^{-} . \qquad (7)$$

Hence, the equilibrium solubility of calcium hydroxide can be written as

$$K_{spl} = \frac{K_{spl}^{o}}{\gamma_{\pm}^{3}} = [Ca^{++}][OH^{-}]^2 , \qquad (8)$$

where K_{spl}^{o} is the thermodynamic solubility product, K_{spl} is the more usual form in which concentrations are used, and the brackets denote solution concentration in molar units. The activity coefficient in Eqn (8), $\gamma_{\pm}$, is dependent on the electrolyte concentration, and accounts for solution nonidealities. Hence, addition of a neutral electrolyte, such as sodium chloride may cause substantial changes in K_{spl} as shown in Fig. 1, which is from the study of Johnson and Grove at ambient temperature (25). There is considerable uncertainty in the literature solubility data for calcium hydroxide. For example, Greenberg, et al. (26) report a solubility product of $9\ (10^{-6})\ M^3$ with no added salt. This is lower than the $3(10^{-5})\ M^3$ value given in Fig. 1. These variations may be attributed to several factors including the influence of particle size and impurities.

The exchange isotherm of Eqn. (6), along with solubility product data, such as in Fig. 1, and the definition of the solubility product in Eqn. (8), constitute the necessary chemistry for handling high pH sodium-calcium ion exchange. Prior to considering the exchange model, however, it is pertinent to discuss briefly the chemistry of orthosilicates.

Since sodium orthosilicate (i.e. $Na_4H_4SiO_4$) is commonly recommended as the alkaline preflush agent (8,9), and since silicate ions will be generated from reservoir silica dissolution in caustic preflushing (27,28), precipitation of calcium silicates may govern the preflush process. The equilibria for hydrated calcium silicate is very complex involving numerous dissolved silicate species and solid solutions of $Ca(OH)_2$ and CaH_2SiO_4 [or $Ca(H_3SiO_4)_2$]. Greenberg and his coworkers (26) suggest that the calcium silicate equilibria for CaO/SiO_2 mole ratios between 1/1 and 1/1.5 may be described by a modification of reaction (7):

$$Ca(OH)_2(s)\ \text{sorbed} \rightleftharpoons Ca^{++} + 2OH^- , \quad (9)$$

combined with calcium silicate formation,

$$CaH_2SiO_4(s) \rightleftharpoons Ca^{++} + H_2SiO_4^{=} . \quad (10)$$

The subscript "sorbed" in Eqn. (9) is written to indicate that hydrated calcium silicates apparently form with calcium hydroxide dispersed through a polymeric silica structure. Some question exists as to whether this is an equilibrium structure (36). In any case, the equilibrium constant for Eqn. (9) is not known. Also, the divalent silicate ion concdntration in Eqn. (10) depends on solution pH. According to Greenberg, et al. (26), the solubility product of reaction (10), K_{sp2},

$$K_{sp2} = [Ca^{++}][H_2SiO_4^{=}] \quad (11)$$

is about 10^{-7} M^2 at 25°C. This is two orders of magnitude lower than the solubility product of calcium hydroxide. However, K_{sp2} remains nearly invariant with increasing temperature (26), whereas calcium hydroxide solubility decreases (25). Consequently, at elevated reservoir temperatures, the differences between K_{sp1} and K_{sp2} will diminish.

Using the simple calcium hydroxide and calcium silicate reactions (7) and (10), and their solubility products, it is possible to calculate the composition of silicate solutions contacting hardness ions. For example, a 1 weight percent sodium orthosilicate solution with a Na_2O/SiO_2 mole ratio of 2/1 will reduce a 1000 ppm calcium solution (i.e. based on the equivalent mass of calcium carbonate) to 1 ppm, and will precipitate calcium silicate. In contrast, a 1 weight percent silicate solution with a Na_2O/SiO_2 mole ratio of 1000/1 will precipitate calcium hydroxide, and reduce the calcium concentration to 10 ppm. In the second case, the initial silicate ion concentration is insufficient to precipitate calcium in the silicate form. This calculation illustrates that although the solubility product for calcium silicate is much lower than that for calcium hydroxide, the calcium hydroxide reaction may dominate. The preferred precipitate form depends on the initial calcium and silicate concentrations. This is an important observation because the molecular form of the calcium precipitate strongly affects preflush efficiency.

In view of the complicated and unquantified chemistry of the silicate system, this paper treats ion exchange with precipitation only for the calcium hydroxide case. In so far as alkaline silicates might be approximated by a single reaction similar to Eqn. (7), then the qualitative features of silicates can be reflected by altering the solubility product, K_{sp1}.

THEORETICAL DEVELOPMENT

Ion Exchange Without Precipitation

Bivariant ion exchange, such as that between sodium and calcium ions, is well understood, and has been discussed by several authors (1-7,8,29). We will review these concepts only so that the analogies between calcium-sodium exchange with calcium hydroxide precipitation and ordinary ion exchange will be apparent. Movement of calcium and sodium ions through an exchanging medium is determined by combining overall and differential species material balances. For the case of equilibrium sodium-calcium exchange without precipitation and dispersion, the two independent material balance equations respectively on, calcium and chloride are as follows:

$$\frac{\partial x}{\partial \tau}\left(1 + \frac{\alpha}{C_s}\frac{dy}{dx}\right) + \frac{\partial x}{\partial \xi} = 0 \quad (12)$$

and

$$\frac{\partial C_s}{\partial \tau} + \frac{\partial C_s}{\partial \xi} = 0 , \quad (13)$$

where

$$\alpha = \rho_s \frac{(1-\phi)Q}{\phi} , \quad (14)$$

and ϕ is the void fraction or porosity, and ρ_s is the solid density. The cation exchange capacity, when adjusted by the solid density and the column porosity, yields the column exchange capacity in equivalents per unit volume of solution, α. Consequently, α/C_s is the ratio of the solid and solution capacities. Position and time variables, z and t, are reduced in the usual fashion by column length, L, and the quotient of column length and the frontal advance rate, $L\phi/u$, to yield ξ and τ.

The calcium material balance, Eqn. (12), admits solution using the method of characteristics (30, 31). For any given salinity and solute equivalent fraction, the solution may be expressed as a calcium concentration velocity:

$$\frac{\xi}{\tau} = \frac{1}{1 + \frac{\alpha}{C_s}\frac{dy}{dx}} . \quad (15)$$

With the mass-action exchange isotherm previously described in Eqn. (6), the solid equivalent fraction, y, increases monotonically with the calcium solution fraction, x. However, the derivative of y with respect to x decreases with increasing x. Consequently, for changes of increasing calcium concentration, the solution represented by Eqn. (15) will be double valued. This physical impossibility is resolved by applying an integral material balance on calcium to determine the velocity of a shock front across which the solid and solute concentrations change abruptly. The resulting shock velocity is

$$\frac{\xi}{\tau} = \frac{1}{1 + \frac{\alpha \Delta y}{\Delta(C_s x)}} \quad , \qquad (16)$$

where Δ indicates differences in the equivalent fractions and salinities between the upstream and downstream side of the shock wave.

Similarly, the solution for the salinity wave demanded by Eqn. (13), is

$$\frac{\xi}{\tau} = 1 \quad . \qquad (17)$$

Because the velocity of the salinity wave is unaffected by its concentration and is equal to the frontal advance rate, salinity waves are often referred to as indifferent. Solute concentrations will be affected by the movement of an indifferent wave in that Δy must equal zero, so that the wave velocities in Eqns. (16) and (17) are each unity. As shown in Eqn. (16), any change in salinity requiring y to be constant will cause the solute fraction, x, to change also.

Injection of a salt solution of salinity C_{ss} and calcium equivalent fraction, x_s, followed by continuous injection of solution at C_{sB} and x_B into a column initially saturated at C_{so} and x_o is solved by requiring Eqns. (15) through (17) to hold at appropriate locations. By way of example, Fig. 2 shows a standard ion exchange history for injection of a 0.25 PV pulse of 0.6 N NaCl followed by continuous injection of 0.5 N NaCl into an exchanging solid substrate (i.e. $\alpha = 0.2$ N, $\beta/C_s = 0.4$ N^{-1}). The solid is initially saturated with 1000 ppm of calcium (on a carbonate mass basis) in a 0.5 N salt solution. Salinity changes cause abrupt transitions at 1.0 and 1.25 pore volumes. If the slug of 0.6 N salt is not introduced, but rather continuous injection of 0.5 N sodium chloride occurs, then the increase in eluted calcium concentration is not observed. The shapes of concentration histories for ion exchange with calcium precipitation will be more complicated.

Ion Exchange with Precipitation

When sodium hydroxide is injected into a column presaturated with a solution containing calcium ions, precipitation of calcium hydroxide occurs, depending on the injected pH and the initial column calcium concentration. Determination of the resultant concentration profiles and histories requires an extension of the classical bivariant ion-exchange theory outlined above. As in exchange without precipitation, the ion-exchange conditions in Eqns. (15) through (17) must be met in the appropriate regions, and bulk solution electroneutrality must be satisfied. If we define C_{OH} as the difference between hydroxide and hydrogen ion concentrations, then Eqn. (18) is the correct statement of electroneutrality:

$$C_s = C_{Na} + C_{Ca} = C_{Cl} + C_{OH} \quad . \qquad (18)$$

In addition, the concentration of hydroxide and calcium must satisfy the solubility relationship of Eqn. (8) in any regions where precipitate exists. As the injected solution moves through the column, two general types of regions are encountered. In the first region type, ion exchange and precipitation are coupled. Consequently, all solute and solid surface concentrations are known, once any two solute or solid concentrations are specified. In the second type of region, calcium and hydroxide concentrations are below their solubility limits and, therefore, are not influenced by precipitation.

In the region where precipitate forms, the solid particles may nucleate either on the rock surfaces or in solution. If nucleated in solution, the precipitated particles will migrate with the pore fluid until captured by solid surfaces. How far the particles move is best described by filtration theory (32). Coupling filtration theory with ion exchange and precipitation is a formidable problem. However, two limiting cases are more readily treated. These are a stationary precipitate (i.e. instantaneous and complete filtration, and/or rock-surface nucleation), and a precipitate moving at the frontal advance rate. Experimental evidence from laboratory column studies (8,9) and arguments about expected particle and pore sizes and reservoir length scales dictate only a stationary precipitate in actual oil recovery processes.

Several additional restrictions of this model include: (1) The ion exchange constant, K_I, is not affected by changes in pH or salinity, (2) The hydroxide ion is not involved in any reactions other than calcium hydroxide precipitation, (3) Precipitation of calcium hydroxide is instantaneous, (4) The precipitate volume is negligible compared to the column void volume, and (5) The solubility product, K_{spl}, is constant, and independent of both pH and salinity. The second assumption is questionable. Its limitations are

discussed later. The constant solubility product restriction is made for mathematical convenience.

To proceed we define a precipitate concentration, p, as the equivalents of calcium hydroxide generated per unit mass of solid exchanger. It is convenient to nondimensionalize p with the cation exchange capacity Q, to give a reduced precipitate concentration, P:

$$P \equiv \frac{p}{Q} \quad . \tag{19}$$

As defined by Eqn. (19), P is the fraction of the total exchange capacity which precipitates and, therefore, must be positive but not greater than unity. If the exchanger is initially saturated with calcium ions, and the precipitate is completely insoluble, then P is identically one.

The assumption of instantaneous precipitation whenever the solubility product is exceeded mandates that all precipitate fronts be abrupt transitions. Extension of the overall material balance Eqn. (16) for calcium to include precipitation yields a wave velocity similar to that of an abrupt transition without precipitation:

$$\frac{\xi}{\tau} = \frac{1}{1 + \frac{\alpha\Delta(y+P)}{\Delta(xC_s)}} \quad . \tag{20}$$

Equation (20), for the calcium concentration velocity when a stationary precipitate forms, differs from Eqn. (16) by the appearance of P. If the precipitate is fully mobile rather than stationary, it constitutes a "solute" rather than a solid concentration, and in Eqn. (20) P then adds to xC_s rather than to y.

Since hydroxide is involved in calcium precipitation, it must be accounted for in the analysis. Consequently, an overall material balance similar to Eqn. (20) is written for hydroxide ions with the following result:

$$\frac{\xi}{\tau} = \frac{1}{1 + \frac{\alpha\Delta P}{\Delta C_{OH}}} \quad . \tag{21}$$

The abrupt changes in hydroxide and calcium concentrations which accompany precipitate formation must occur simultaneously. That is, the wave velocities defined by Eqns. (20) and (21) must be equal so that,

$$\frac{\Delta(y+P)}{\Delta(C_s x)} = \frac{\Delta P}{\Delta C_{OH}} \quad . \tag{22}$$

This condition, referred to as coherence, is the tendency of concentrations constituting a given composition to travel with the same wave velocity.

Two final classifications need to be established in the theory. We distinguish between precipitates that instantaneously redissolve and those that do not upon contact with a solution of concentration below the solubility limit. The statement of nonredissolution implies a nonequilibrium state, which only occurs if the rate of precipitate dissolution is small relative to the residence time of the solution in the column. The converse holds for the opposite redissolution case. Because of the vast length scales in reservoirs compared to laboratory columns, nonredissolution may be appropriate in the laboratory, but redissolution will be expected in field applications.

A nonredissolution situation is computationally simpler because calcium hydroxide, once precipitated, is then inert and has no further effect on ion exchange. Mathematical solution of this case involves first the indifferent salinity wave governed by Eqn. (17), with the accompanying condition of $\Delta y = 0$. Equation (22), along with the exchange isotherm and the solubility product, determines the amount of calcium hydroxide precipitated. The velocity of the precipitate wave follows from Eqn. (20) [or from Eqn. (21)]. Behind the precipitate front Eqns. (15) - (17), for ion exchange without precipitation, apply.

For the instantaneous redissolution situation, where column residence time is large compared to the dissolution rate, calculations are more difficult. They differ from the nonredissolution case above in that Eqns. (20) - (22) in combination with the exchange isotherm and the solubility product specify the amount of precipitate generated, and the velocities of both the precipitate and redissolution waves. Eqns. (16) and (17) apply in zones where precipitate is present, provided that hydroxide and calcium concentrations upstream and downstream of the abrupt transitions satisfy the solubility product. Eqns. (15) - (17), for ion exchange without precipitation, again control in the zones behind the redissolution wave where precipitate is no longer present.

In the next section, we present theoretical concentration histories for continuous and pulse injection of sodium hydroxide into a calcium-loaded exchanger. We examine these cases for either no redissolution of precipitated calcium hydroxide or instantaneous redissolution. The interested reader will find the detailed calculation procedures outlined in Appendices A and B, which also present characteristic diagrams and selected concentration profiles.

THEORETICAL CALCULATIONS

Figures 3 through 10 give the results of the theoretical calculations for a sample sodium-calcium exchanging solid. The exchange parameters, α and β/C_s, are given in Table 1. They correspond to a cation exchange capacity of 3.5 mequivalents per 100 grams of solid and an exchange constant, K_I,

of 0.014 cm^3/gram for a void fraction and solid density of 0.3 and 2.5 grams/cm^3, respectively.

The selected column presaturation conditions are a salinity of 0.5 N and a calcium equivalent fraction of 0.10. A calcium hydroxide solubility product, K_{spl}, of 5 (10^{-5}) M^3 and an invariant chloride ion concentration of 0.5 N are assumed. In addition, the solution following finite pulses of sodium hydroxide solution is neutral, as is the solution initially in place.

In Figs. 3 - 10, the calcium ion concentration, given for convenience in ppm of $CaCO_3$, is designated by a solid line. The pH histories are shown as dotted lines. The calcium profile for the neutral pH situation (i.e. continuous injection of NaCl at 0.5 N) has been included for reference, and is indicated by a dashed line. That is, the dashed line corresponds to the simple softened brine ion exchange shown previously in Fig. 2. Slug size and inlet pH are specified in each plot as τ_s and pH_s, respectively.

Continuous Alkali Injection

Figures 3 through 6 are effluent histories when sodium hydroxide is injected continuously as designated by $\tau_s = \infty$. The no redissolution and redissolution results for an injection pH of 13.0 are presented in Figs. 3 and 4. Analogous computations for an injection pH of 12.7 are given in Figs. 5 and 6.

Calcium concentration and pH are at their presaturation values for time less than one pore volume. At one pore volume, the added presence of hydroxide ions increases the solution salinity and requires a corresponding abrupt increase in the effluent calcium ion concentration (see Fig. 2 for comparison). Formation of calcium hydroxide reduces the pH eluting directly after one pore volume. The extent of this reduction is not influenced by the injection pH. Rather, the pH and calcium concentration in this zone depend on the calcium presaturation concentration, the ion exchange isotherm, and the solubility product (see Appendices A and B for details). The second abrupt transition at about 1.5 pore volumes is generated by the calcium hydroxide precipitation front.

If the precipitated calcium is not considered to redissolve, then the total mass of calcium ions which appears in the effluent is reduced by the amount precipitated. Thus, for the no redissolution cases, Figs. 3 and 5, the areas beneath the solid curves are less than the areas under the dashed, simple ion-exchange curves. Since a lower hydroxide concentration precipitates less calcium, longer times are required to remove calcium ions (compare Figs. 3 and 5). Thus, if the precipitate does not redissolve, increasing the pH decreases the time required to reduce calcium elution concentration to zero. Clearly, Figs. 3 and 5 reveal that for a non-redissolving precipitate, continuous injection of sodium hydroxide more efficiently removes calcium ions than does a softened brine. In addition, this calcium removal efficiency increases with increasing injected pH.

If redissolution of calcium hydroxide occurs, as in Figs. 4 and 6, then conservation of mass forces the area below the dashed and solid curves to be equal. From Fig. 4, for an injection pH of 13.0, we discover that calcium hydroxide precipitation quickly reduces the effluent calcium ion concentration to a low plateau value, but that calcium production continues at this low concentration for a longer time than for simple ion exchange. If the injection pH is reduced to 12.7, as in Fig. 6, less calcium is precipitated and its removal is sooner than for simple ion exchange. The greater solubility of calcium hydroxide in a pH 12.7 solution than in a pH 13.0 solution causes a higher plateau concentration and a faster redissolution wave. The precipitate dissolution wave is produced at 2.4 pore volumes for the pH 12.7 solution, but not until 5.3 pore volumes (not shown in Fig. 4) for the pH 13.0 solution.

Precipitate redissolution causes the pH of the solution in contact with the precipitate zone to be greater than the injection pH. For example, the second plateau pH in Fig. 4 is 13.03. Consequently, the calcium solution concentration in the precipitate zone is lower in the redissolution case than for the counterpart case of no redissolution in Fig. 3.

For continuous alkali injection with precipitate redissolution shown in Figs. 4 and 6, we find that high pH solutions are initially more efficient in removing calcium than are softened brines. However, at sufficiently high pH, complete calcium removal from the reservoir rock will occur earlier with a standard softened brine. Obviously, as the injected pH is lowered, the efficiency of both alkali and softened brines become similar.

Pulse Alkali Injection

Figures 7 through 10 show effluent histories of finite pulses of sodium hydroxide in 0.5 N sodium chloride followed continously by neutral 0.5 N sodium chloride. Figures 7 and 8 are for no redissolution of the precipitate. Figures 9 and 10 include the effects of redissolution. As for the continuous injection diagrams, calcium is reported in equivalent calcium carbonate concentration and denoted with a solid line. A dotted line indicates hydroxide effluent concentration. The dashed line represents the calcium response for continuous injection of neutral 0.5 N sodium chloride (i.e. ion exchange without precipitation). The presaturation solution is the same as for the continuous alkali injection. Pulse sizes are

denoted by a dimensionless pore-volume duration, τ_s, and all pulseshave an injection pH of 13.

We examine first the no redissolution classification shown in Figs. 7 and 8. For the 0.25 PV alkaline slug in Fig. 7, the effluent hydroxide never reaches the inlet pH value of 13. This occurs because for relatively small pulses of hydroxide the slug back overtakes the slower precipitate-forming slug front. When wave overlap takes place in the column, no additional calcium hydroxide precipitates. Furthermore, the inlet high pH pulse is reduced to an equilibrium level which depends on the initial calcium concentration, the ion exchange isotherm, and the solubility product.

For a larger slug, as in Fig. 8, the pulse back does not overtake the precipitation wave, so calcium is precipitated over the entire column length. Thus, the maximum amount of calcium is precipitated, and complete removal of calcium in the effluent to a zero concentration takes only slightly longer than for the continuous injection case in Fig. 3. This situation applies to the 0.5 PV alkaline pulse in Fig. 8, and is recognized by some of the effluent hydroxide remaining at the injected pH.

The effluent plateau concentration of calcium corresponding to the precipitate region is less for the finite pulse examples (Figs. 7 and 8) than for the infinite pulse case (Fig. 3). The explanation resides in the lower hydroxide concentration of the solution following the slug, which requires a lower ionic strength exchange isotherm, and hence, a lower calcium concentration. Likewise, the slightly more efficient calcium removal for continuous injection as compared to the larger pulsed injection results mainly from the presence of additional hydroxide ions which increase the solution salinity. Thus, when no redissolution takes place, the benefit of continuous pH injection can be obtained with a finite pH pulse, provided that the pulse is large enough to prevent wave overlap, and is chased by a softened brine of salinity equal to (or greather than) the high pH solution.

Figures 9 and 10 show the behavior of pulsed alkaline preflushing when the precipitate instantaneously redissolves. The noteworthy feature, as compared to the continuous injection case of Fig. 4, is the high calcium pulse. With the conditions in Figs. 9 and 10, the increased calcium concentration exceeds the initial value in the column. The origin of the high calcium concentration pulse is the redissolution of solid calcium hydroxide into a lower pH solution, which can accommodate larger amounts of calcium according to the solubility relation, Eqn. (8). Such redissolution zones of high calcium concentration, not previously recognized (8, 9), have potentially severe consequences for alkaline preflushing. Oil recovery chemicals following the alkaline slug may encounter higher divalent ion concentrations than originally in the reservoir. Since the zone of high calcium concentration in Figs. 9 and 10 is rather narrow, it will, of course, be spread by dispersion, which is not included in the present treatment.

To alleviate somewhat the calcium redissolution pulse, larger alkaline pulses may be employed. Increasing the injected volume, τ_s, of the high pH solution from 0.25 PV in Fig. 9 to 1.0 PV in Fig. 10 delays and decreases the volume of the high calcium concentration pulse. With continuous alkali injection, as in Fig. 4, the volume of the delayed calcium slug is zero. This continuous injection limit is approached if the pulse of high pH solution is large enough so that the softened brine salinity wave following the pulse, and the redissolution wave do not interfere.

Discussion

From the theoretical calculations presented in Figs. 3 through 10, the most desirable performance of alkaline preflushing is anticipated when the precipitate does not redissolve, the alkaline pulse size is large, and the solubility product of the precipitate is very low. We amplify each of these factors below.

Unfortunately, in a field application of alkaline preflushing, it is not likely that the divalent ion precipitate remains insoluble in the low pH region behind the alkaline pulse. The rate of solid precipitate dissolution depends on a concentration driving force, and mass transfer and/or kinetic resistances. Inclusion of such finite dissolution kinetics into the present model will introduce (for a first order reaction) the dimensionless Damköhler number, $Da = kL/u$, where k is either a mass transfer or kinetic rate coefficient (28). The no redissolution limit is approached when the Damköhler number is very small. Conversely, when the Damköhler number is very large the instantaneous redissolution limit emerges. Reservoir lengths are large resulting in large Damköhler numbers. Hence, the complete redissolution calculation illustrated in Figs. 4, 6, 9, and 10 are appropriate in field applications.

Preliminary column experiments in our laboratory, when compared with available literature correlations (33), indicate that solid calcium hydroxide dissolution is mass transfer limited. Thus, for laboratory experiments of alkaline calcium-sodium ion exchange, we conclude that the no redissolution calculation should better approximate the measurements. However, nonredissolution is most likely precluded in oil reservoirs.

As noted earlier, redissolution theory predicts that increasing pulse size delays and decreases the volume of the high calcium concentration zone at the back of the alkaline slug. If the redissolution wave velocity is designated as $(\xi/\tau)_{3Pb}$, then the alkaline

pulse case approaches the continuous injection calcium removal efficiency when the slug size, τ_s, satisfies the following inequality:

$$\tau_s \equiv \frac{1-(\xi/\tau)_{3Pb}}{(\xi/\tau)_{3Pb}} \quad . \qquad (23)$$

Equation (23) states mathematically that the alkaline pulse must be large enough to prevent interference between the redissolution wave and the pulse back. The meaning of the subscript 3Pb is described in Table 2 and in Appendices A and B.

Figures 3 through 10 reveal that the precipitate reduced calcium concentrations are not extremely low even at relative high pH values of around 13. The calcium hydroxide solubility product, especially in brine, is not low enough. Hence, sodium hydroxide alone does not appear to be a promising preflushing agent. However, when caustic and sufficient silicate are used in conjunction, there does appear to be more promise.

At the alkaline silicate front, where calcium silicates and hydroxides precipitate according to reactions like those in Eqns. (9) and (10), a lower solubility than for calcium hydroxide is likely, depending on the unquantified effects of reservoir temperature, and salinity. At the rear of the alkaline silicate pulse, the precipitate will attempt to dissolve. Here the effect of pH on the solubility product, K_{sp2}, must be considered. Specifically, silicate ion solubility in neutral solutions is low according to the silica reaction,

$$SiO_2(s) + 2OH^- \rightleftharpoons H_2SiO_4^= \quad . \qquad (24)$$

So, if equilibrium is approached in the low pH region following an alkaline pulse, hydrated calcium silicate redissolves releasing calcium ions and precipitating silica.

The appropriate solubility product, K_{sp3}, for the effect of pH on the redissolution of calcium silicate is obtained by combining Eqn. (11) and the equilibrium constant expression from Eqn. (24):

$$K_{sp3} = [Ca^{++}][OH^-]^2 \quad . \qquad (25)$$

This solubility product controls the velocity of the redissolution wave of the low pH solution following the alkaline pulse. From the known equilibrium constant of reaction (24) [i.e. about 10^{-4} M^{-1}(26)] and K_{sp2}, its value is approximately 10^{-11} M^3 at 25°C, or about six orders of magnitude lower than that for calcium hydroxide. Consequently, the high calcium concentration pulse seen in Figs. 9 and 10 for calcium hydroxide is substantially reduced if calcium silicate is precipitated instead. Thus, we speculate that calcium silicate precipitation will yield a consistently lower calcium ion concentration for a longer period of time than will calcium hydroxide.

EXPERIMENT AND RESULTS

Column tests were performed on a solvent extracted Wilmington oil sand (19,28) at 25°C, and at a constant flow rate of 1.5 μm/sec (0.4 ft/day). The original unconsolidated core material is packed into a 33 cm long by 3.8 cm I.D. stainless steel core holder. The core is copiously extracted with Chevron 410H solvent followed by isopropyl alcohol, and then dried to constant weight in a vacuum oven. It is then vacuum saturated with a 1 weight percent solution (0.173 N) of NaCl in distilled and deionized water. Saturation with the sodium chloride solution continues until the inlet and outlet concentrations are identical.

To determine the sodium-calcium ion exchange isotherm, neutral solutions of 0.173 N calcium chloride or sodium/calcium chloride mixtures are introduced and effluent samples collected until calcium breakthrough occurs. Calcium concentrations are measured by EDTA titration (28). After each introduction of calcium, the oil sand is restored to its sodium form by extensively flushing with sodium chloride until no calcium ions are detected in the effluent.

Figure 11 shows the experimental exchange isotherm for the particular Wilmington oil sand examined. The exchange capacity, Q, is around 2 mequivalent/100 g (28). A best-fit solid line is drawn according to the mass action isotherm of Eqn. (6). The resulting isotherm parameters are given in Table 1. They are needed for the ion exchange with precipitation calculations outlined below.

To provide verification of the ion exchange with precipitation model the Wilmington oil sand is first loaded with 0.173N calcium chloride. Once constant column presaturation is achieved, continuous injection of 0.110 N sodium hydroxide in 1 weight percent sodium chloride commences, and effluent samples are collected and analyzed for calcium and hydroxide ion concentration. Hydroxide concentrations are measured by either glass electrodes or by HCl titration to a potentiometric end point.

Calcium and hydroxide effluent responses are shown in Figs. 12 and 13, respectively. Using the measured sodium-calcium ion exchange isotherm in Fig. 11 and Table 1, profiles are calculated for a solubility product, K_{sp1}, of 10^{-4} M^3 (short dashed line) and 10^{-5} M^3 (solid line). Since the dissolution of calcium hydroxide is, as noted previously, mass transfer limited relative to the column residence time, we use the non-redissolution theory in these two figures.

Clearly, the hydroxide increase and concomitant calcium increase is later than predicted by theory. This is anticipated since hydroxide is known to reversibly exchange with this sand (28) causing an additional chromatographic delay. When no precipitation occurs the reversible sodium-hydrogen exchange reaction alone postpones hydroxide production of a pH 13.04 solution by approximately 0.3 pore volumes (28). If this delay, denoted as τ_H, is included in the theoretical calculations, the resultant predictions are also shown in Figs. 12 and 13 for calcium hydroxide solubility products of 10^{-4} M^3 (dotted line) and 10^{-5} M^3 (long dashed line). In Fig. 13, the dotted and long dashed lines first follow the ion exchange without precipitation prediction (dot-dashed line for pH = 7) up to about 1.5 pore volumes. Incorporation of the sodium-hydroxide exchange delay brings the theoretical predictions and experimental results into much closer agreement. The slight discrepancy of the calcium history in Fig. 12 is most likely due to errors in the original sodium-calcium exchange isotherm in Fig. 11. Hence, for continuous caustic injection into a Wilmington oil sand, the proposed theory is satisfactory.

Campbell presents results of similar experiments but for finite pulses of alkali in Berea cores (8). The core dimensions were 5x5x61 cm and the flow rate was 4.8 μm/sec. Unfortunately, Campbell does not report the sodium-calcium exchange isotherm for his Berea cores. We, therefore, chose to fit a calcium effluent history with the mass action exchange isotherm and Eqn. (15) for continuous injection of 3 weight percent sodium chloride. The calcium history (8) and the calculated best fit are shown in Fig. 14. Isotherm exchange parameters are listed in Fig. 14 and and in Table 1. A value of α equal to 0.033 N corresponds to a cation exchange capacity of about 0.5 mequivalent/100 g in basic agreement with the findings of Smith for Berea (2).

Negligigle exchange interaction of hydroxide is expected with the lower surface area Berea sandstones. Hence, the isotherm found from Fig. 14 and the proposed ion-exchange theory with precipitation permit prediction of Campbell's pulsed alkaline preflushes. Again, for the laboratory experiments, the no redissolution subcase of the theory is applied.

Calcium and hydroxide effluent responses and theoretical comparisons are shown in Figs. 15 through 18 for 0.1 PV and 0.25 PV pulses of 0.125 normal sodium hydroxide in a 3 weight percent sodium chloride solution. In Figs. 15 and 16, the calcium history is seen to agree very well with the model when the calcium hydroxide solubility product is taken as 10^{-5} M^3. This solubility product is lower than that reported in Fig. 1 for 0.5 normal sodium chloride solutions. The reason for the lower K_{spl} value is not clear. There may be some influence of soluble silicates produced by reaction with the quartz content of the rock (28). This trend toward the smaller solubility is apparent in both Campbell's and our own data in Figs.12 and 13.

Prediction of the hydroxide effluent concentrations is shown in Figs. 17 and 18. The experimental hydroxide data are not reported in reference (8) and were made available by Campbell (34). Agreement between theory and data for hydroxide is not as succesful as for calcium. Experimental values do not reach the computed peak concentrations and then decline to neutral. Rather, a steady plateau of hydroxide is established at a concentration between 10^{-4} and 10^{-5} N. At this plateau the corresponding calcium effluent concentration is undetectable by EDTA titration. Constant production of a small amount of hydroxide suggests slow dissolution of precipitated calcium hydroxide. For a pH of 10 the calcium content from calcium hydroxie dissolving stoichiometrically would be only 10 ppm, and hence, not detectable in Figs. 15 and 16. Presumably the high peak hydroxide concentrations, which are predicted to be narrow by the theory, have been spread by dispersion. Thus, when examined closely by the sensitive pH measurements, rate effects appear in the laboratory experiments and the asymptotic limit of complete nonredissolution is not reached.

CONCLUSIONS

1. Classical equilibrium bivariant ion exchange theory is extended to include alkaline precipitation of hardness ions. Both continuous and finite pulse injection are considered. Continuous alkali injection removes calcium most efficiently. The minimum pulse size required to approximate continuous injection depends on the initial presaturation, the ion-exchange equilibrium, the solubility product, and the pH of both the pulse and the solution following the pulse.

2. Laboratory column tests can be easily misapplied in field predictions. In particular, very little precipitated material redissolves for laboratory column lengths and frontal advance rates. However, at field lengths and flow rates, precipitate redissolution will probably be complete.

3. Some concentration pulses are narrow and will be strongly affected by dispersion, which is not included in this model.

4. Alkaline preflushes for hardness cation removal prior to low pH micellar or polymer solutions are not attractive if cation hydroxide is precipitated. The relatively high solubility of calcium hydroxide permits large concentrations of calcium ions to occur when low pH solutions contact the precipitated material.

5. If sufficient silicate ions are present in the alkaline preflush and equilibrium

exists, calcium ion removal may be dominated by silicate precipitation. Hydrated calcium silicate has a very low solubility in low pH solutions and the calcium concentration of the redissolution pulse is much less than for calcium hydroxide.

6. The theory agrees reasonably well with experimental results both for continuous and pulse injection of alkali. For the Wilmington sand chromatographic delay of hydroxide caused by reversible sodium-hydrogen ion exchange (or surface hydroxylation) must be included.

NOMENCLATURE

C_{Ca} = calcium ion concentration, equiv/dm^3
C_{Cl} = chloride ion concentration, equiv/dm^3.
C_{Na} = sodium ion concentration, equiv/dm^3.
C_{OH} = hydroxide ion concentration, equiv/dm^3.
C_s = salinity, sum of calcium and sodium ion concentrations, equiv/dm^3.
Da = kL/u, Damköhler number
k = dissolution rate constant, sec^{-1}.
K_I = sodium-calcium ion-exchange equilibrium constant, dm^3/g.
K_{sp1} = solubility product for reaction (8), M^3.
K_{sp2} = solubility product for reaction (11), M^3.
K_{sp3} = solubility product for reaction (25), M^3.
L = column length, m
M = molarity, mol/dm^3
M = mineral exchanged site
N = normality, equiv/dm^3.
p = precipitate concentration, equiv/dm^3.
P = p/Q, reduced precipitate concentration.
ppm = parts per million
ppt = precipitate
PV = pore volumes
q_{Ca} = calcium ion exchanged sites, mequiv/100g.
q_{Na} = sodium ion exchanged sites, mequiv/100g.
Q = cation exchange capacity, mequiv/100g.
s = solid
t = time, s
T = temperature, °C
u = superficial velocity, m/s
x = calcium equivalent fraction of solution
y = calcium equivalent fraction of solid
z = axial position, m

Greek Symbols

α = $\rho_s(1-\phi)Q/\phi$, reduced cation exchange capacity.
β = $K_I C_s/Q$, dimensionless sodium-calcium exchange constant.
$\gamma_{\pm}$ = activity coefficient
Δ = difference operator.
ξ = z/L, reduced column length
ρ_s = solid density, g/cm^3.
τ = ut/ϕL, pore volume
τ_H = sodium-hydrogen exchange delay, pore volume
ϕ = porosity

Subscripts

B = solution following the finite pulse
b = back of zone denoted in characteristic diagrams (see Table 2)
C = constant calcium concentration zone as denoted in characteristic diagrams (see Table 2)
c = position or time denoted in characteristic diagram (see Fig. 23)
f = front of zone denoted in characteristic diagrams (see Table 2)
i = position or time denoted in characteristic diagram (see Fig. 23)
P = precipitate zone as denoted in characteristic diagrams (see Table 2)
P = position or time denoted in characteristic diagrams (see Figs. 21 and 23)
s = slug solution
T = transition zone as denoted in characteristic diagrams (see Table 2)
o = initial presaturation conditions
0 - 7 = numerals denoting zones in the characteristic diagram (see Table 2)

Superscripts

i = intermediate equivalent fraction in a transition zone
o = maximum equivalent fraction in a transition zone.

ACKNOWLEDGEMENT

This work was performed with financial support from the Department of Energy on Contract # W-7405-ENG-48 with the Lawrence Berkeley Laboratory of the University of California. The authors are grateful to Dr. Robert Berg for his encouragement and participation in technical discussions. The efforts of J. MacGlashan are acknowledged in aiding in the experiments. Thanks are given to Dr. T. Campbell for releasing unpublished data.

REFERENCES

1. Hill, H. J., Helfferich, F. J., Lake, L. W., Reisberg, J. and Pope, G. A.: "Cation Exchange and Chemical Flooding," J. Pet. Tech., (Oct. 1977), 1336.

2. Smith, F. W.: "Ion Exchange Conditioning of Sandstones for Chemical Flooding," J. Pet. Tech., (June 1978), 959.

3. Hill, H. J. and Lake, L. W., "Cation Exchange-Chemical Flooding Experiments," SPE 6770, presented at 52nd Annual Fall Technical Conference, Denver, CO, Oct. 10-12, 1977.

4. Griffith, T. D.: "Application of the Ion Exchange Process to Reservoir Preflushes," SPE 7587, presented at 53rd Annual Fall Technical Conference, Houston, TX, Oct. 1-3, 1978.

5. Lake, L. W. and Helfferich, F. G.: "The Effect of Dispersion, Cation Exchange, and Polymer/Surfactant Adsorption on Chemical Flood Environment," SPE 6769, presented at 52nd Annual Fall Technical Conference, Denver, CO, Oct. 10-12, 1977.

6. Pope, G. A., Lake, L. W. and Helfferich, F. G.: "Cation Exchange in Chemical Flooding--Basic Theory without Dispersion," SPE 6771, presented at 52nd Annual Fall Technical Conference, Denver, CO, Oct. 10-12, 1977.

7. Chiou, C. S. and Chang, H. L.: "Preflood Design for Chemical Flooding-- A Study on Ion Exchange/Dispersion Processes in Porous Media, Paper 37b, presented at AIChE 84th National Meeting, Atlanta, GA, Feb. 26-Mar. 1, 1978.

8. Campbell, T. C.: "Chemical Flooding: A Comparison Between Alkaline and Soft Preflushed Systems for Removal of Hardness Ions from Reservoir Brines," SPE 7873, presented at Symposium on Oil Field and Geothermal Chemistry, Houston, TX, Jan. 22-24, 1979.

9. Holm, L. W. and Robertson, S. D.: "Improved Micellar-Polymer Flooding with High pH Chemicals," SPE 7583, presented at 53rd Annual Fall Technical Conference, Houston, TX, Oct. 1-3, 1978.

10. Gary Operating Co., "Bell Creek Field Micellar-Polymer Pilot Demonstration," 2nd Annual DOE Report, Oct. 1977-Sept. 1978. DOE-BETC-1802-27.

11. Cooke, C. E., Jr., Williams, R. E. and Kolodzie, P. A.: "Oil Recovery by Alkaline Waterflooding," J. Pet. Tech., (Dec. 1974), 1365.

12. Jennings, H. Y., Jr., Johnson, C. E., Jr. and MacAuliffe, C. D.: "A Caustic Waterflooding Process for Heavy Oils," J. Pet. Tech., (Dec. 1974), 1344.

13. Johnson, C. E., Jr.: "Status of Caustic and Emulsion Methods," J. Pet. Tech., (Jan. 1976), 85.

14. Ehrlich, R. and Wygal, R. J." "Interrelation of Crude Oil and Rock Properties with the Recovery of Oil by Caustic Waterflooding," SPE J (Aug. 1977), 233.

15. Carmichael, J. D., Mayer, E. H., Alpay, O. A. and Boyle, P. R.: "Caustic Waterflooding Demonstration Project, Ranger Zone, Long Beach Unit, Wilmington Field, Calif.," 4th DOE Symposium on Enhanced Oil and Gas Recovery and Improved Drillings Methods, Tulsa, OK, Aug. 29-31, 1978; 5th DOE Symposium on Enhanced Oil and Gas Recovery and Imporved Drilling Methods, Tulsa, OK, Aug. 22-24, 1979.

16. Emery, L. W., Mungan, N. and Nicholson, R. W.: "Caustic Slug Injection in the Singleton Field," J. Pet. Tech., (Dec. 1970), 1569.

17. Mayer, E. H., Berg, R. L., Carmichael J. D. and Weinbrandt, R. M., "Alkaline Injection for Enhanced Oil Recovery - A Status Report," SPE 8848, presented at 1st Joint SPE/DOE Symposium on Enhanced Oil Recovery, Tulsa, OK, April 20-23, 1980.

18. Raimondi, P., Gallagher, B. J., Bennett, G. S., Ehrlich, R. and Messner, J. H.: "Alkaline Waterflooding Design and Implementation of a Field Pilot," SPE 5831, Presented at SPE Symposium on Improved Oil Recovery, Tulsa, OK, March 22-24, 1976.

19. Radke, C. J. and Somerton, W. H.: "Enhanced Recovery with Mobility and Reactive Tension Agents," 4th Annual DOE Symposium on Enhanced Oil and Gas Recovery and Improved Drilling Methods, Tulsa, OK, Aug. 29-31, 1978; 5th Annual DOE Symposium on Enhanced Oil and Gas Recovery and Improved Drilling Methods, Tulsa, OK, Aug. 22-24, 1979.

20. Page, B. W.,: "Theory of Precipitation Ion Exchange with Application to Calcium Hydroxide Desalting," Ph. D. Thesis, Univ. Calif., Berkeley (1971).

21. Golden, F.: "Theory of Fixed-Bed Performance for Ion Exchange Accompanied by Chemical Reaction," Ph. D, Thesis, Univ. Calif., Berkeley (1973); Golden, F., Shiloh, K. I., Klein, G. and Vermeulen, T.: "Theory of Ion-Complexing Effects on Ion-Exchange Column Performance," J. Phys. Chem. (1974), 78, 926.

22. Klein, G.: Unplublished report, 1971.

23. Page, B. W., Klein, G., Golden, F. and Vermeulen, T., "Mixed-Bed Ion Exchange Desalting by the Calcium Hydroxide Process," AIChE Symposium Series, Vol. 71, No. 152 (1975).

24. van Bladel, R., Gavira, G. and Laudelout, H.: "A Comparison of the Thermodynamic, Double Layer Theory and Empirical Studies of the Na-Ca Exchange Equilibrium in Clay-Water Systems," Proc. International Clay Conference (1972), 385-398.

25. Johnson, J. and Grove, C.: "The Solubility of Calcium Hydroxide in Aqueous Salt Solutions," J. Am. Chem. Soc., (1931), 53, 3976-91.

26. Greenberg, S. A., Chang, T. N. and Anderson, E.: "Investigation of Colloidal Hydrated Calcium Silicates. I. Solubility Products," J. Phys. Chem., (Sept. 1960), 64, 1151; Greenberg, S. A., and Chang T. N.: "Investigation of the Colloidal

Hydrated Calcium Silicates. II. Solubility Relationships in the Calcium Oxide - Silica-Water System at 25°C," J. Phys. Chem., (Jan. 1965), 69 (1), 182.

27. Reed, M. G.: "Gravel Pack and Formation Sandstone Dissolution During Steam Injection," SPE 8424, presented at 54th Annual Technical Conference, Las Vegas, NV, Sept. 23-26, 1979.

28. Somerton, W. H. and Radke, C. J.: "Role of Clays in Enhanced Recovery of Petroleum," SPE 8845, presented at First Joint SPE/DOE Symposium on Enhanced Oil Recovery, Tulsa, OK, April 20-23, 1980.

29. Helfferich, F.: "Ion Exchange," McGraw-Hill, NY, (1962),

30. Aris, R. and Amundson, N. R.: "First Order Partial Differential Equations with Applications," Prentice-Hall, Englewood Cliffs, NJ (1973).

31. Acrivos, A., "Method of Characteristics Technique," Ind. Eng. Chem., (1956), 48, 703-10.

32. Herzig, J. P., Leclerc, D. M. and LeGoff, P.: "Flow of Suspensions through Porous Media - Application to Deep Bed Filtration," Ind. Eng. Chem., (1970), 62, 8.

33. Fedkiw, P. and Newman, J.: "Low Peclet Number Behavior of the Transfer Rate in Packed Beds," Chem. Engr. Sci., (1978).

34. Iler, R. K.: "The Chemistry of Silica," Wiley, NY (1979).

35. Steinour, H. H.: "Preceedings of the 3rd International Symposium on the Chemistry of Cement, London, (1952).

APPENDIX A: CHARACTERISTIC DIAGRAMS AND CONCENTRATION PROFILES

Characteristic Diagrams

To aid in the mathematical solution it is useful to construct characteristic diagrams corresponding to constant chemical composition displayed in a position-time (ξ-τ) space. The slope of these lines represents the composition wave velocity (ξ/τ).

Figures 19 through 23 are generalized characteristic diagrams which illustrate, in a qualitative fashion solutions for the five cases discussed in this paper: ion exchange without precipitation, continuous pH injection with and without precipitate redissolution, and finite pulse injection with and without redissolution. For all of these plots, the calcium equivalent fraction of the pulse and solution following it are zero.

To clarify these figures, the various concentration regions have been labelled and summarized in Table 2. Specifically, zones of constant salinity and pH are denoted with the same arabic numerals (0-7). Within these numbered regions are subzones for which the calcium ion concentration is constant (indicated by a C), gradually changing (a gradual transition indicated by a T) or constant and influenced by the presence of precipitation (indicated by a P). Ion the region marked 0, initial column conditions exist. Occasionally, more than one transition or constant subzone exists for a single numbered salinity zone, so these are distinguished by numeric subscripts.

A graphical convention indicates the type of transition which occurs between these various zones and subzones. Thus, gradual transitions are denoted by dotted lines. Likewise, solid lines represent the salinity (or indifferent) wave where the calcium solute transition is abrupt and satisfies the condition of constant solid equivalent fraction (i.e. $\Delta y = 0$). Lines of long dashes represent the precipitate formation wave across which an abrupt transition occurs satisfying Eqns. (20) and (21). Compound transitions composed of the juxtaposition of abrupt and gradual portions are appropriately plotted as dot-dashed lines. Such compound transitions occur when the precipitate redissolution wave velocity given by Eqns. (20) and (21) and the beginning of the gradual transition zone from Eqn. (15) coincide. Lines of short dashes denote abrupt transitions of the type satisfying Eqn. (16).

Figure 19 shows the standard ion-exchange characteristic diagram for a salinity pulse of duration τ_s when no precipitation occurs. Since the solute concentrations of the solid-preferred ion, calcium, is decreasing (i.e. no calcium is injected), only gradual transitions and abrupt salinity-induced transitions are observed. The pulse salinity (C_{ss}) exists in zone 1, while the salinity following the slug (C_{sB}) exists in zone 4. The calcium concentration in both the $1C_1$ and $4C_1$ subzones is equal to the injection value, which is zero in this example. The characteristic diagram in Fig. 19 may be compared to the calcium concentration history in Fig. 2 in the main text.

Figure 20 is a generalized characteristic plot for continuous injection of sodium hydroxide in which a precipitate forms, but does not redissolve. Two abrupt transitions result; the first due to a salinity change and the second due to precipitate formation.

Calcium and hydroxide concentrations at the location of the precipitate front (long dashed line) depend on the solubility product, because the solution is in contact with the solid calcium hydroxide . Additional constraints are the presaturation conditions and the ion-exchange equilibrium. Normally, this fixes the concentrations in zone 1. However, for certain combinations of column presaturation conditions, the injected solution concentrations, and the solubility product, the concentration velocity computed from Eqn. (15) for the zone 1 concentrations is greater than the precipitate front velocity given by

Eqn. (20). By induction we conclude that ion exchange cannot occur prior to the precipitate front. If the zone 1 concentrations are in equilibrium according to Eqn. (8), and ion exchange occurs prior to the precipitate fornt, then the requirement that all solutions contacting solid $Ca(OH)_2$ be in equilbirum cannot be met. Conversely, if the solute concentrations at the abrupt precipitate transition are in equilbirium, any ion exchange in advance of this front means an increase in the calcium ion concentration above the solubility limit. Consequently, the concentrations in zone 1 are constant and determined from only the presaturation condition, the solubility product, and the feed chloride concentration. Appendix B presents the governing equations in more detail. For this case of no precipitate redissolution, ion exchange behind the precipitation producing front proceeds as for the case without precipitation.

Figure 21 is a characteristic plot when sodium hydroxide is injected for a finite number of pore volumes, τ_s, and when no redissolution of the precipitate is permitted. Solute concentrations in zone 1 are the same as for the continuous injection case of Fig. 20. The salinity and hydroxide concentration in zone 2 are at the injection concentration of the finite pulse (C_{ss}, C_{OHs}). In zone 4, they are the concentrations behind the pulse (C_{sB}, C_{OHB}). The precipitate front (long dashed line) moves at the same velocity as the continuous injection case. However, at some time and position (τ_p, ξ_p) the back of the hydroxide pulse over takes the precipitate front. Hence, precipition no longer occurs. Thus, following slug elution, precipitate is present only at positions less than ξ_p.

The generalized characteristic diagram for continuous injection of sodium hydroxide and instantaneous redissolution of the precipitate is shown in Fig. 22. There are a number of similarities to the continuous nonredissolution case in Fig. 20. However, because the precipitate redissolves when it is contacted by fresh solution a zone (3P) of constant composition is created in which precipitate is generated in the front and dissolve in the back. For many combinations of column presaturation, ion-exchange equilibrium, and solubility product, the precipitate redissolution wave is a compound transition whose velocity is determined by simultaneously satisfying Eqn. (15), (20), and (21). For other combinations of process conditions, the precipitate may be so sparingly soluble that the redissolution wave moves very slowly, and no gradual transition zone (2T) exists. As for the no redissolution example in Fig. 20, the 2C zone is in equilibrium with the injected calcium concentration and salinity.

Figure 23 presents the characteristic plot for finite pulse injection of sodium hydroxide when redissolution is allowed. Within the region of the two salinity waves, designated by solid lines, the concentrations and velocities are the same as for infinite injection of hydroxide in Fig. 22. In the region behind the slug, four zones of constant salinity and hydroxide concentration exist. These zones, marked 4 through 7, will all have the same chloride ion concentration as the solution following the pulse. The salinity and hydroxide ion concentration of zone 4 is the same as the solution injected following the high pH pulse (C_{sB}, C_{OHB}).

In zones 5 and 6, precipitate is present and, therefore, the solubility equation applies. Since the calcium equivalent fraction on the solid in zone 6 must equal that of zone 3 (i.e. $\Delta y = 0$) and the chloride concentration is known, all other compositions are fixed. In particular, if the chloride concentration is the same for the high pH slug and the solution following the slug, then the composition of zones 3 and 6 will be identical. This requires concentrations in zone 1 and 7 to also be equivalent, since they must satisfy the same set of conditions.

The reduced pH of the solution following the finite pulse of alkaline water allows this solution to hold a higher calcium ion concentration. This can generate a concentration shock front (denoted by short dashed lines) from a lower to higher calcium ion concentration separating the precipitate zones 5 and 6. Zone 5 has a higher calcium ion concentration than zone 6. Because solubility equilibrium exists in both zones, the hydroxide concentration of zone 5 is therefore less than zone 6. The velocity of this calcium shock wave (short dashed lines), which originates at location (τ_c, ξ_c), is given by Eqn. (16). The velocity of the precipitate dissolution wave between zones 5 and $4T_2$ satisfies Eqns. (15), (20) and (22), simultaneously, just as for the 3P-2T front.

Under certain combinations of process variables the velocity of the precipitate dissolution wave between zones $4T_2$ and 5 may exceed the shock front and zone 5 will not exist In instances when the injected pH and presaturation calcium ion concentration are not much greater than their solubility limits, the precipitate dissolution wave in the region behind the finite pulse may even overtake the precipitate generation front. When this happens no further precipitation takes place.

Concentration Profiles

Use of the characteristic diagrams is illustrated by showing concentration profiles for various column throughputs in the same example system described in the theoretical calculation section of the main text. Only finite pulses of alkali are described, since continuous injection is a straightforward simplification. Pulse profiles also demonstrate the importance of slug size, and how the various zones increase or decrease in size as they move through the column. Concentration profiles represent a vertical line on the characteristic plot; that is, they display

graphicaly the variation of concentration with position for a fixed time.

Figures 24 through 29 portray calcium and hydroxide concentration profiles at several times for a 0.25 PV pulse of pH 13.0 solution. Figures 24-26 are for the no redissolution case; precipitate dissolution is demonstrated in Figs. 27-29. As in previous figures, calcium and hydroxide concentrations are designated with solid and dotted lines, respectively. Included for reference is the calcium profile when no precipitation occurs (i.e. standard ion exchange) plotted as a dashed line. The region in which precipitate is present is also indicated.

The profile after 0.25 PV of fluid has been injected and no redissolution occurs is shown in Fig. 24. At this time injection of neutral solution following the slug has not begun. Thus, the profile is the same as for the continuous injection of pH 13.0 solution. The high pH zone has progressed to 0.17 pore volumes. Once the injection of neutral solution behind the slug begins, the volume of the high pH zone decreases. After 0.75 PV is injected Fig. 25 reveals that the region of high pH has diminished to 0.02 PV. It entirely disappears in Fig. 26 when 1.0 PV of solution has been injected.

In Fig. 25 the first abrupt decrease in calcium concentration (i.e. $\xi \sim 0.53$) results from precipitate formation. The next concentration drop (i.e. $\xi \sim 0.5$ PV) is caused by a pH and consequent salinity decrease. At some time between the injection of 0.75 and 1.0 pore volumes, as shown in Figs. 25 and 26, the pulse back overtakes the precipitation wave. The time and position at which this occurs is identified in the characteristic plot in Fig. 21 as τ_p and ξ_p. After τ_p pore volumes is injected, no further precipitation takes place. Precipitate is present then only at positions less than ξ_p. This is the situation in Fig. 26; the amount of precipitate remains unchanged in the region of of ξ less than 0.56.

Figure 27 is a plot of the resultant concentration profiles after 0.25 pore volumes of solution is injected and instantaneous redissolution occurs. As in Fig. 24, no neutral solution following the slug has yet entered the column. Therefore, Fig. 27 is the same as for the continuous injection case. As discussed already, precipitate redissolution causes the pH in the precipitate region (i.e. $.05 < \xi < 0.17$) to be slightly greater than the injected value.

The larger solubility of calcium hydroxide in the nonalkaline solution which follows the high pH pulse causes an abrupt increase in the calcium solute concentration. This is shown in Fig. 28 where the front of the zone of increased calcium is at $\xi = 0.17$. After 1.0 PV of sodium hydroxide is injected, Fig. 29 reveals that the high calcium front has progressed to $\xi = 0.44$, and the zone has widened somewhat. The higher $Ca(OH)_2$ solubility in neutral solution means that the precipitate wave velocity is relatively fast. Thus, the high calcium concentration zone remains reasonably narrow. Clearly dispersion, neglected in these calculations, will be important here.

The alkaline preflush shown in the example calculations of Figs. 27 through 29 (or Figs. 9 and 10 of the text) would not be effective. High concentrations of calcium ions are introduced behind the hydroxide pulse where interference with micellar and/or polymer solutions is likely. In this example, simple ion exchange removes all calcium over a larger region than does the alkaline pulse.

APPENDIX B: DETAILED COMPUTATIONS

We illustrate the computational procedure for the finite pulse, no redissolution case, since the other cases represent simplifications. Known are the presaturation conditions (x_o, y_o, C_{so}, C_{OHo}, C_{Clo}), the pulse concentrations (x_s, C_{ss}, C_{OHs}) and size (τ_s), and the concentrations of the solution following the pulse (x_B, C_{SB}, C_{OHB}). For convenience, we again assume that no additional calcium is injected (i.e. $x_s = x_B = 0$) and that constant chloride ion concentration is maintained ($C_{Clo} = C_{Cls} = C_{ClB}$). Concentrations and wave velocities are determined for each zone by satisfying Eqns. (8), (15) - (18), (20), and (22) in the appropriate regions.

Since zone 1 borders an indifferent wave, Δy must be zero. In addition, solution electroneutrality and solubility product equations apply. Thus, the concentrations in zone 1 are determined by simultaneous solution of Eqns. (B1) through (B3):

$$y_1 = y\,(C_{s1}, x_1) = y_o \qquad \text{(B1)}$$

$$C_{s1} = C_{OH1} + C_{Cls} \quad , \qquad \text{(B2)}$$

$$C_{s1} x_1 C_{OH1}^2 = 2K_{sp1} \quad . \qquad \text{(B3)}$$

The ion exchange isotherm in Eqn. (B1) expressed explicitly for y, is dependent on both the salinity and calcium solution equivalent fraction. At high pH the hydroxide concentration, $[OH^-]$, can be replaced by C_{OH}.

Concentrations in the precipitate zone, 3P, depend on both the precipitate and redissolution wave velocities. Thus, Eqns. (20), (21) and (22) are required to fully specify this region. Solution salinity and hydroxide concentration of zone 2 are the same as the injected solution (i.e $C_{s2} = C_{ss}$ and $C_{OH2} = C_{OHs}$). Once zone 1 concentrations are known, zone 3 and zone 2 conditions are computed by simultaneously satisfying the following seven conditions:

$$y_3 = y\,(C_{s3}, x_3) \quad , \qquad \text{(B4)}$$

$$y_2 = y\ (C_{ss},\ x_2^o) \quad , \tag{B5}$$

$$C_{s3} = C_{OH3} + C_{Cls} \quad , \tag{B6}$$

$$C_{s3}x_3\ C_{OH3}^2 = 2K_{spl} \quad , \tag{B7}$$

$$\left.\frac{\tau}{\xi}\right|_{3Pf} = 1 + \frac{\alpha(P+y_3-y_1)}{C_{s3}x_3 - C_{s1}x_1} = 1 + \frac{\alpha P}{C_{OH3}-C_{OH1}} \quad , \tag{B8}$$

$$\left.\frac{\tau}{\xi}\right|_{3Pb} = 1 + \frac{\alpha P}{C_{OH3}-C_{OH2}} = 1 + \frac{\alpha(P+y_3-y_2)}{C_{s3}x_3 - C_{ss}x_2} \quad , \tag{B9}$$

$$\left.\frac{\tau}{\xi}\right|_{3Pb} = \left.\frac{\tau}{\xi}\right|_{2Tf} = 1 + \frac{\alpha}{C_{ss}}\frac{dy}{dx}\ (C_{ss}, x_2^o) \quad . \tag{B10}$$

The velocities of the front and back of the 3P zone are presented in these relations as $\left.\frac{\xi}{\tau}\right|_{3Pf}$ and $\left.\frac{\xi}{\tau}\right|_{3Pb}$, respectively. The velocity for the maximum calcium equivalent fraction (x_2^o) in the gradual transition zone, 2T, is denoted by the subscript 2Tf.

Equation (15) determines concentration velocities for intermediate solution equivalent fractions ($x_2^o \geq x_2^i \geq 0$) in the transtional zone, 2T,

$$\left.\frac{\xi}{\tau}\right|_{2T^i} = \frac{1}{1 + \frac{\alpha}{C_{ss}}\frac{dy}{dx}\ (C_{ss}, x_2^i)} \quad . \tag{B11}$$

Computation of concentrations and velocities of the zones behind the pulse follow essentially the same procedure, except that the point of wave generation occurs at finite values of τ and ξ instead of the origin as it does for zones within the slug. In particular, zones 5P and $4T_2$ originate from (τ_c, ξ_c) which is calculated from Eqn. (B12):

$$\tau_c = \xi_c + \tau_s = \frac{\tau_s}{1 - \left.\frac{\xi}{\tau}\right|_{3Pb}} \quad . \tag{B12}$$

The conditions which must be satisfied between zones 1C and 7C as well as between 3P and 6P are the same as for 1C and 0. For constant chloride concentration, zone 1C and 7C concentrations are equivalent, as are zones 6P and 3P, and therefore,

$$\left.\frac{\tau - \tau_p}{\xi - \xi_p}\right|_{7Cb} = \left.\frac{\tau - \tau_p}{\xi - \xi_p}\right|_{6Pf} = \left.\frac{\tau}{\xi}\right|_{3Pf} \quad , \tag{B13}$$

where $$\tau_p = \xi_p + \tau_s = \frac{\tau_s}{1 - \left.\frac{\xi}{\tau}\right|_{3Pf}} \quad . \tag{B14}$$

The subscripts of 7Cb and 6Pf denote the boundaries at the back of the 7C and front of the 6P zones.

Concentrations in zone 5P and the maximum equivalent fraction ($x_{4,2}^o$) in the gradual transition zone, $4T_2$, are computed from Eqns. (B15) - (B22). That is, we require the following:

$$\left.\frac{\tau - \tau_c}{\xi - \xi_c}\right|_{5Pf} = \left.\frac{\tau - \tau_c}{\xi - \xi_c}\right|_{6Pb} = 1 + \frac{\alpha(y_6 - y_5)}{C_{s6}x_6 - x_5C_{s5}} \tag{B15}$$

$$\left.\frac{\tau - \tau_c}{\xi - \xi_c}\right|_{5Pb} = \left.\frac{\tau - \tau_c}{\xi - \xi_c}\right|_{4T_2f} = 1 + \frac{\alpha}{C_{sB}}\frac{dy}{dx}\ (C_{sB}, x_{4,2}^o), \tag{B16}$$

$$\left.\frac{\tau - \tau_c}{\xi - \xi_c}\right|_{5Pb} = 1 + \frac{\alpha P}{C_{OH5}-C_{OHB}} = 1 + \frac{\alpha(P+y_5-y_{4,2}^o)}{C_{s5}x_5 - C_{sB}x_{4,2}^o}, \tag{B17}$$

$$y_5 = y\ (C_{s5},\ x_5) \quad , \tag{B18}$$

$$y_{4,2}^o = y\ (C_{s4,2}, x_{4,2}^o) \quad , \tag{B19}$$

$$C_{s5} = C_{Cl1B} + C_{OH5} \quad . \tag{B20}$$

As in zone 2, the hydroxide concentration and salinity in zone 4 is the same as the injected solution ($C_{OH4} = C_{OHB}$ and $C_{s4} = C_{sB}$).

The maximum equivalent fraction of calcium in zone $4T_1$ ($x_{4,1}^o$) which is also the minimum calcium equivalent fraction in zone $4T_2$, is determined by satisfying Eqn. (B21):

$$y_{4,1}^o = y\ (C_{sB},\ x_{4,1}^o) = y_2^o = y\ (C_{ss},\ x_2^o). \tag{B21}$$

Thus, the calcium ion concentration in zone $4T_2$ ($x_{4,1}^i$) decreases from $x_{4,2}^o$ to $x_{4,1}^o$ according to Eqn. (B22):

$$\left.\frac{\tau - \tau_c}{\xi - \xi_c}\right|_{4T_2^i} = 1 + \frac{\alpha}{C_{sB}}\frac{dy}{dx}\ (C_{sB},\ x_{4,1}^i) \tag{B22}$$

In zone $4T_1$, the concentration velocities as the calcium equivalent fraction is depleted from $x_{4,1}^o$ to zero, are determined from

Eqns. (B23) through (B25).

$$\left.\frac{\tau-\tau_i}{\xi-\xi_i}\right|_{4T^i} = 1 + \frac{\alpha}{C_{sB}}\frac{dy}{dx}\left(C_{sB},\ x^i_{4,1}\right) \qquad \text{(B23)}$$

$$y^i_{4,1} = y\left(C_{sB},\ x^i_{4,1}\right) = y^i_2 = y\left(C_{ss}, x^i_2\right) \qquad \text{(B24)}$$

$$\tau_i = \xi_i + \tau_s = \frac{\tau_s\left[1 + \frac{\alpha}{C_{ss}}\frac{dy}{dx}\left(C_{ss}, x^i_2\right)\right]}{\frac{\alpha}{C_{ss}}\frac{dy}{dx}\left(C_{ss}, x^i_2\right)} \qquad \text{(B25)}$$

This completes the problem. Concentration profiles or effluent histories are obtained by either examining concentrations at positions, ξ, for a fixed value of τ or of fixing ξ at unity and determining concentrations at various times, τ.

TABLE 1

Sodium-Calcium Exchange Isotherm Parameters

Solid	α (N)	β/C_s (N^{-1})
Calculation	0.2	0.4
Wilmington	0.142	0.35
Berea (Campbell)	0.033	0.0030

TABLE 2

Characteristic Diagram Regions

Zone	Description	Subzone	Description
0	presaturation	none	none
1	precipitate reduced pH and salinity	C_2, C	salinity induced calcium concentration change
		C_1	pulse calcium concentration
		T	ion-exchange gradual transition
2	pulse pH and salinity	C_2	precipitate reduced calcium concentration
		C_1	pulse calcium concentration
		T	ion-exchange gradual transition
3P	precipitate increased pH and salinity, precipitate reduced calicum	None	None
4	salinity and pH of solution behind the pulse	C_3	salinity induced calcium concentration change
		C_2	salinity induced calcium concentration change
		C_1	injected solution calcium concentration
		T_2	ion-exchange gradual transition
		T_1	salinity induced calcium concentration change and ion exchange gradual transition
5P	precipitate increased pH and salinity, precipitate reduced calcium	None	None
6P	precipitate increased pH and salinity, redissolution increased calcium	None	None
7P	precipitate reduced pH and salinity	None	None

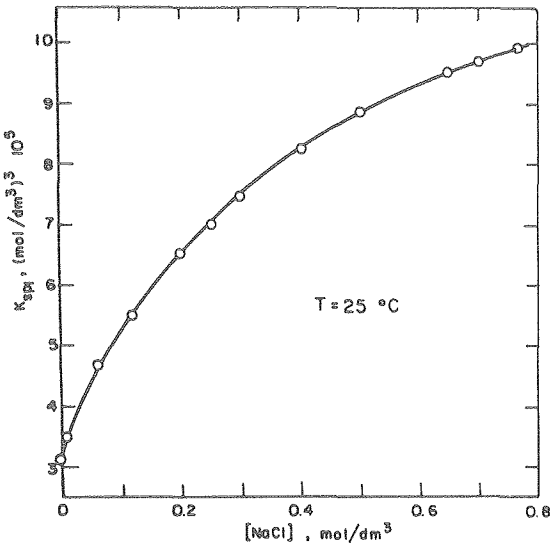

Fig. 1 - Effect of NaCl concentration on the solubility product of calcium hydroxide.

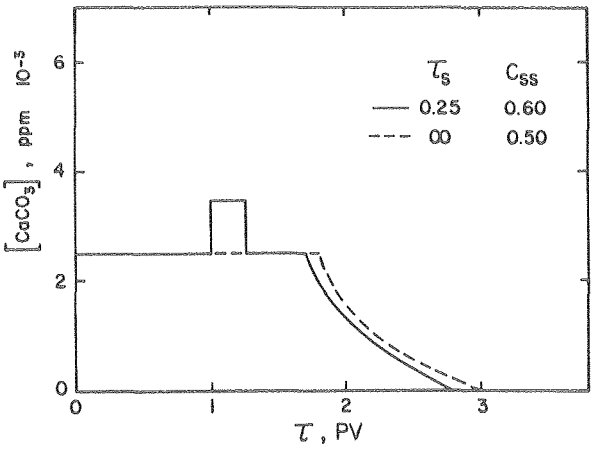

Fig. 2 - Calcium history for neutral NaCl solutions.

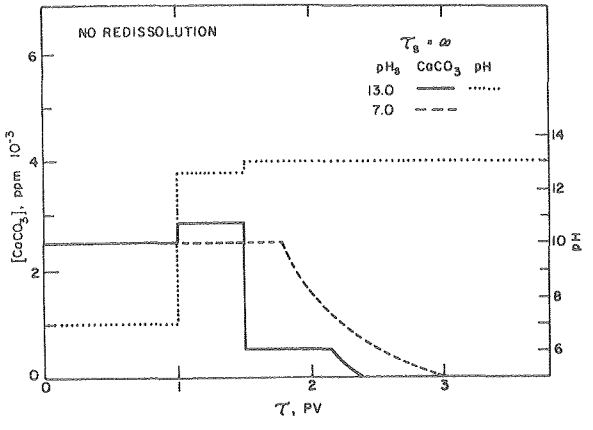

Fig. 3 - Effluent history for continuous alkali injection at pH 13.0 and no redissolution of precipitate.

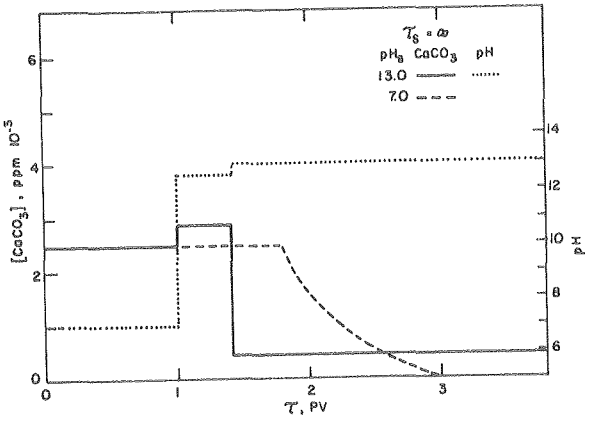

Fig. 4 - Effluent history for continuous alkali injection at pH 13.0 and equilibirum precipite redissolution.

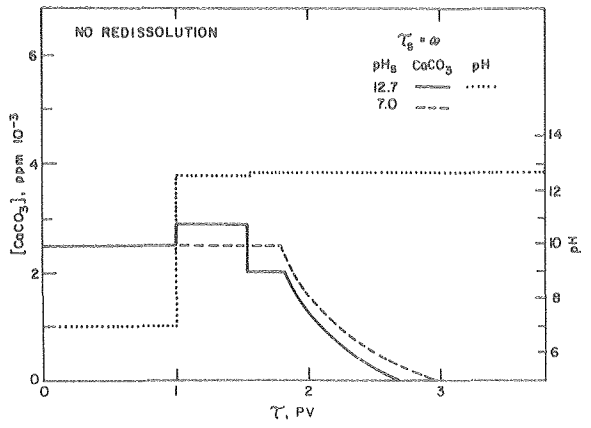

Fig. 5 - Effluent history for continuous alkali injection at pH 12.7 and no redissolution of precipitate.

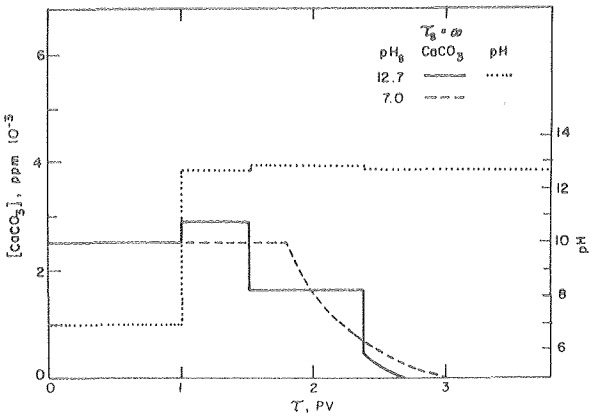

Fig. 6 - Effluent history for continuous alkali injection at pH 12.7 and equilibrium precipitate redissolution.

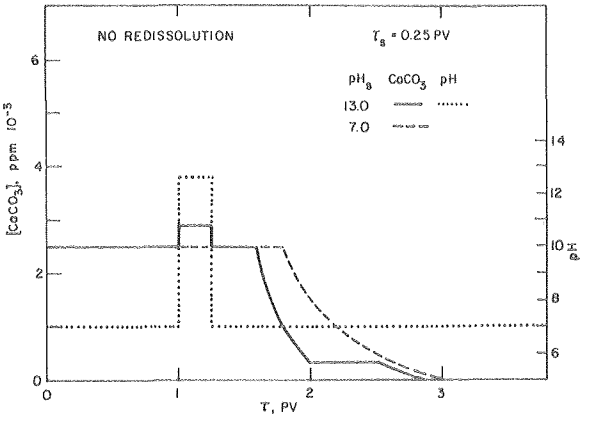

Fig. 7 - Effluent history for 0.25 PV alkali pulse injection at pH 13.0 and no redissolution of precipitate.

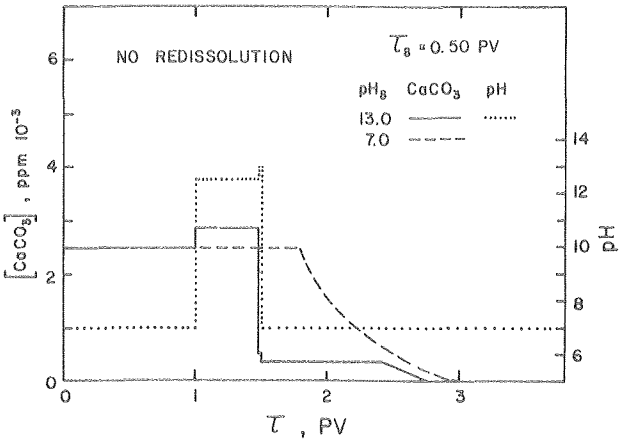

Fig. 8 - Effluent history for 0.50 PV alkali pulse injection at pH 13.0 and no redissolution of precipitate.

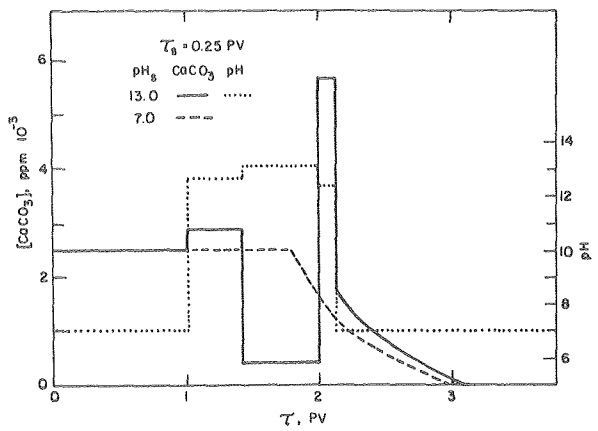

Fig. 9 - Effluent history for 0.25 PV alkali pulse injection at pH 13.0 and equilibrium precipitate redissolution.

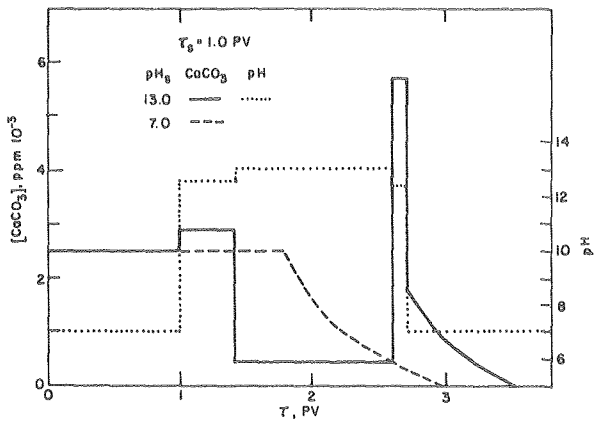

Fig. 10 - Effluent history for 1.0 PV alkali pulse injection at pH 13.0 and equilibrium precipitate redissolution.

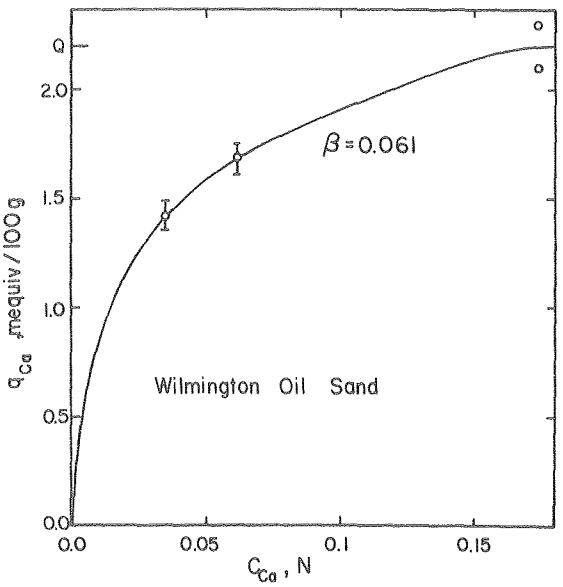

Fig. 11 - Sodium-calcium equilibrium exchange isotherm for Wilmington oil sand at 25°C.

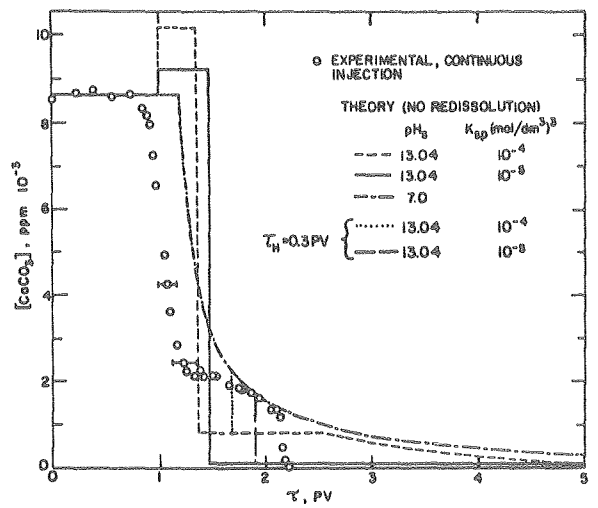

Fig. 12 - Experimental results and theoretical predictions of calcium response for continuous alkali injection at pH 13.04 into a calcium saturated Wilington oil sand at 25°C.

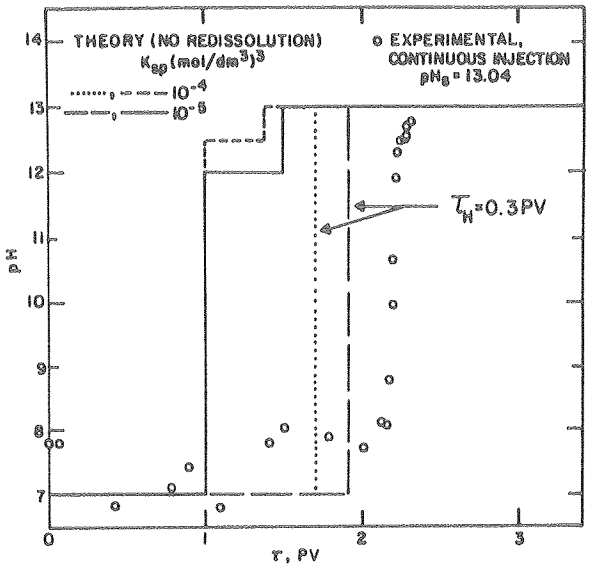

Fig. 13 - Experimental results and theoretical predictions of pH response for continuous alkali injection at pH 13.04 into a calcium saturated Wilmington oil sand at 25°C.

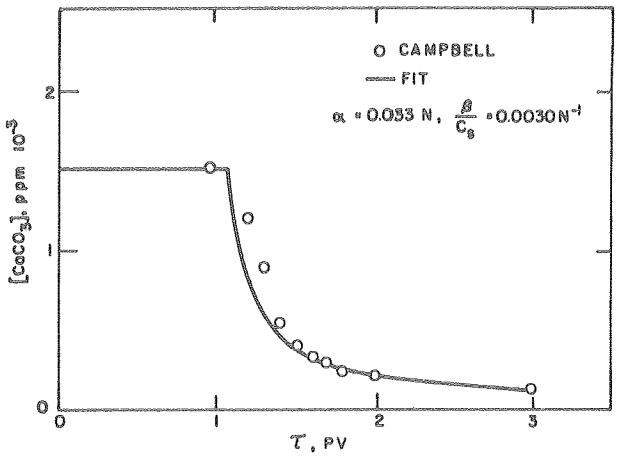

Fig. 14 - Fit of calcium response of Berea sandstone for neutral 3 weight percent NaCl solution at 25°C.

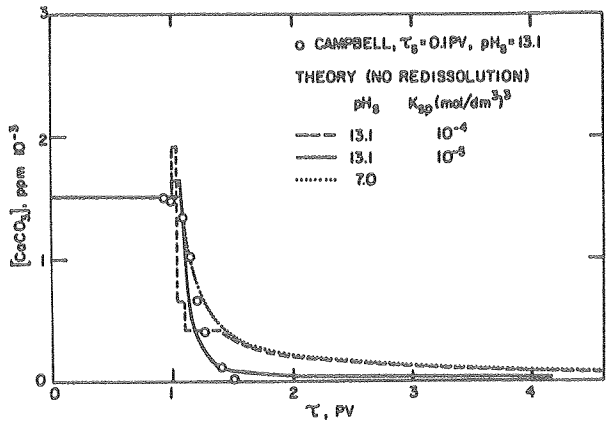

Fig. 15 - Campbell's results and theoretical predictions of calcium response for 0.1 PV alkali pulse injection at pH 13.1 into Berea sandstone at 25°C.

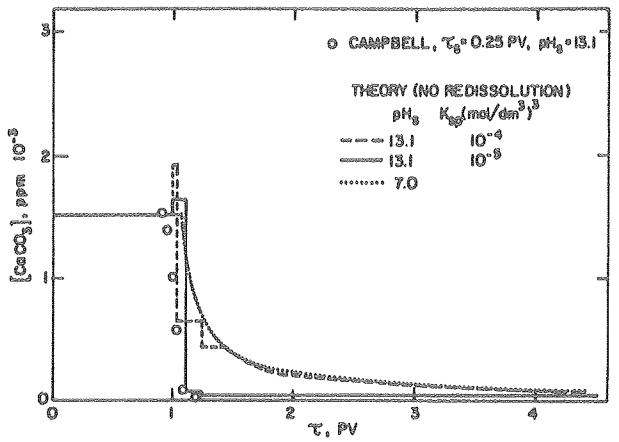

Fig. 16 - Campbell's results and theoretical predictions of calcium response for continuous 0.25 PV alkali pulse injection at pH 13.1 into Berea sandstone at 25°C.

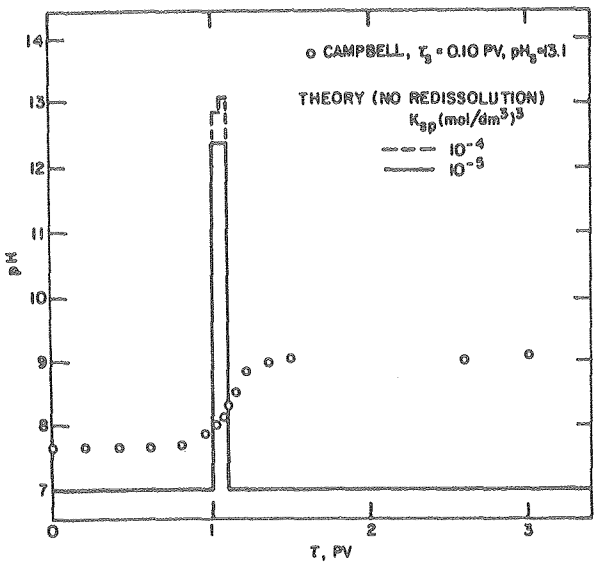

Fig. 17 - Campbell's results and theoretical predictions of pH response for 0.1 PV alkali pulse injection at pH 13.1 into Berea sandstone at 25°C.

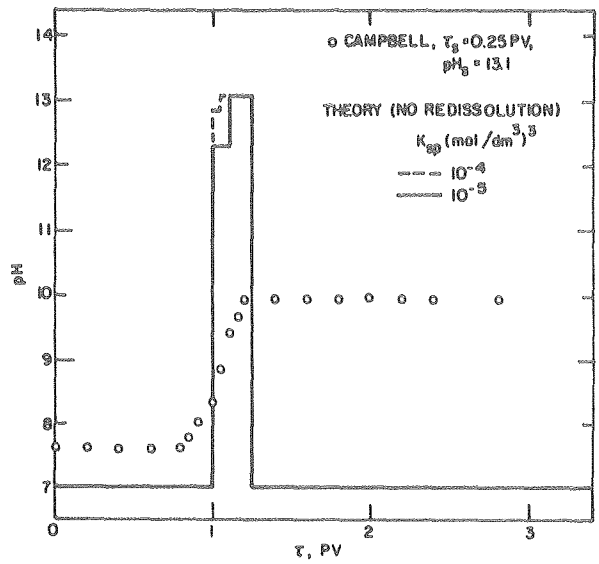

Fig. 18 - Campbell's results and theoretical predictions of response for 0.25PV alkali pulse injection at pH 13.1 into Berea sandstone at 25°C.

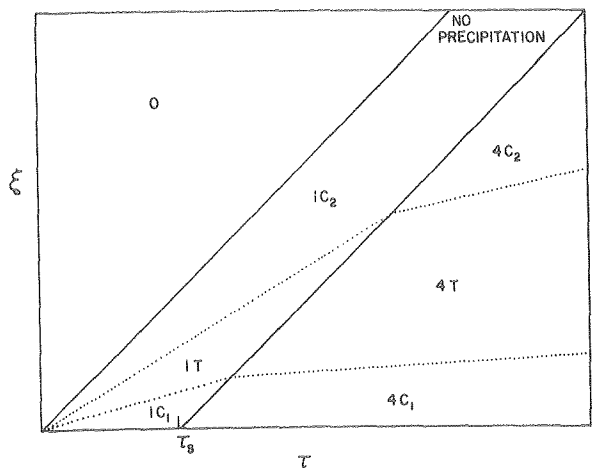

Fig. 19 - Generalized ξ-τ characteristic diagram for injection of a τ_s PV pulse of neutral NaCl solution.

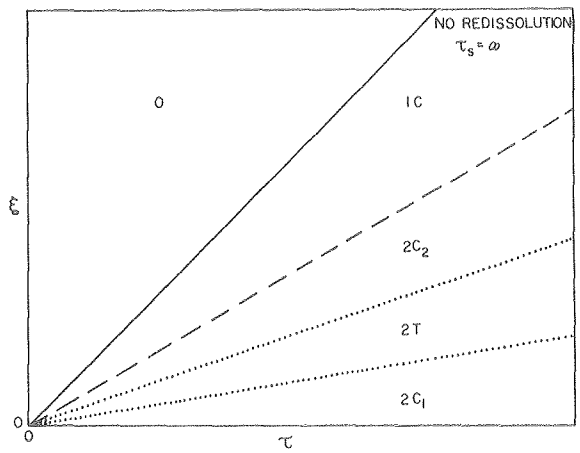

Fig. 20 - Generalized ξ-τ characteristic diagram for continuous injection of alkali and no redissolution of precipitate.

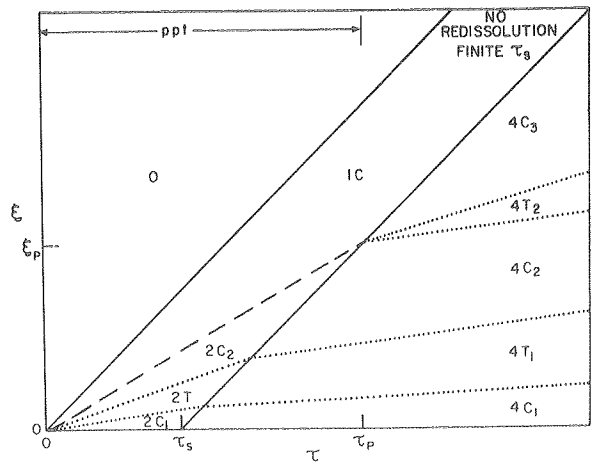

Fig. 21 - Generalized $\xi-\tau$ characteristic diagram for a τ_s PV pulse injection of alkali and no redissolution of precipitate.

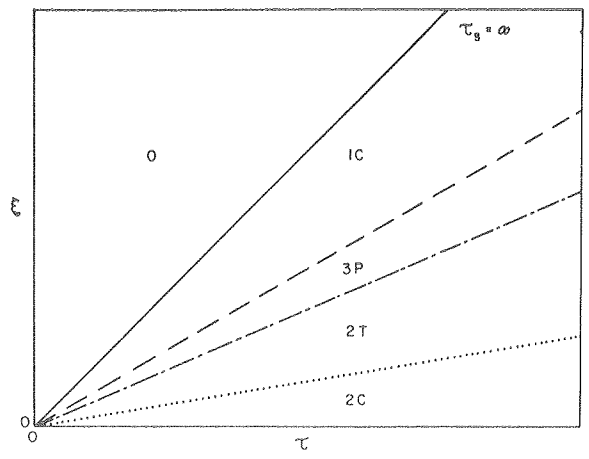

Fig. 22 - Generalized $\xi-\tau$ characteristic diagram for continuous injection of alkali and equilbirium precipitate redissolution.

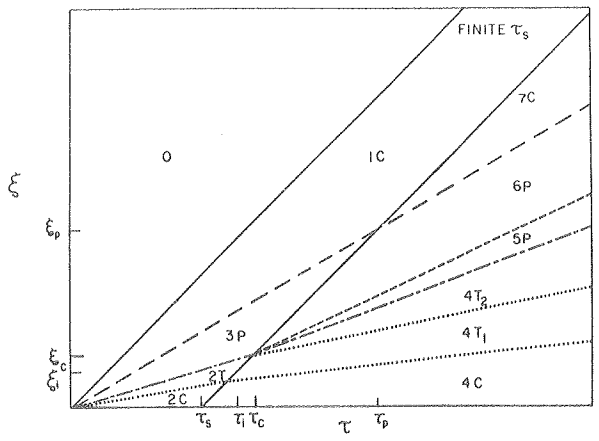

Fig. 23 - Generalized $\xi-\tau$ characteristic diagram for a τ_s PV pulse injection of alkali and equilibrium precipitate redissolution.

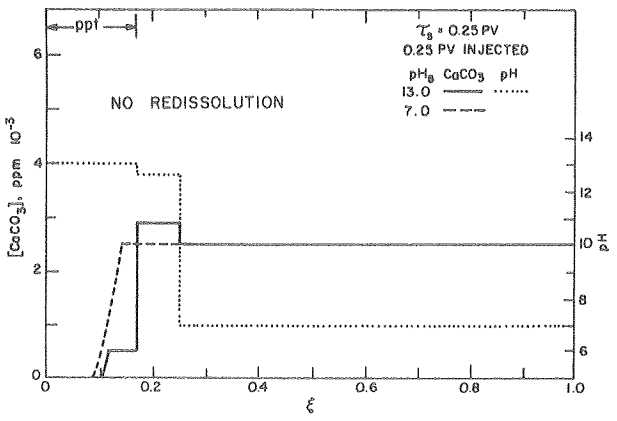

Fig. 24 - Concentration profiles after τ = 0.25 PV for 0.25 PV alkali pulse injection of pH 13.0 and no precipitate redissolution.

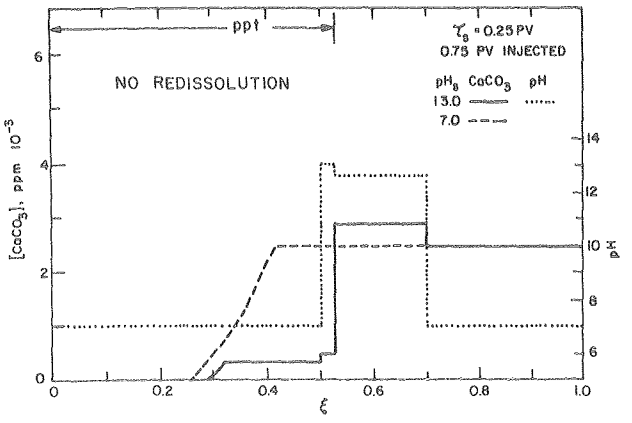

Fig. 25 - Concentration profiles after τ = 0.75 PV for a 0.25 PV pulse injection of pH 13.0 and no precipitate redissolution.

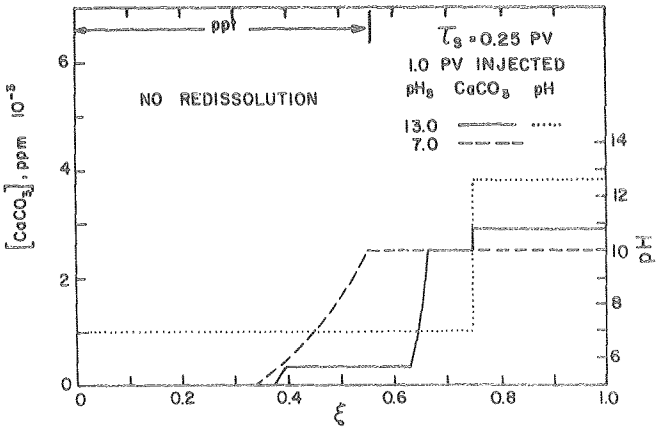

Fig. 26 - Concentration profiles after τ = 1 PV pulse injection of pH 13.0 and no precipitate redissolution.

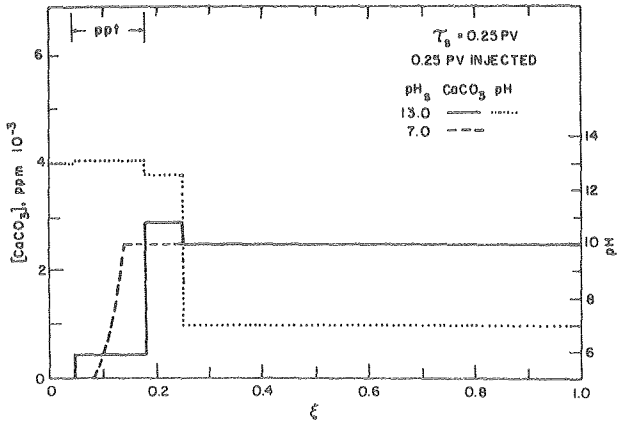

Fig. 27 - Concentration profiles after τ = 0.25 PV for a 0.25 PV pulse injection of pH 13.0 and equilibrium precipitate redissolution.

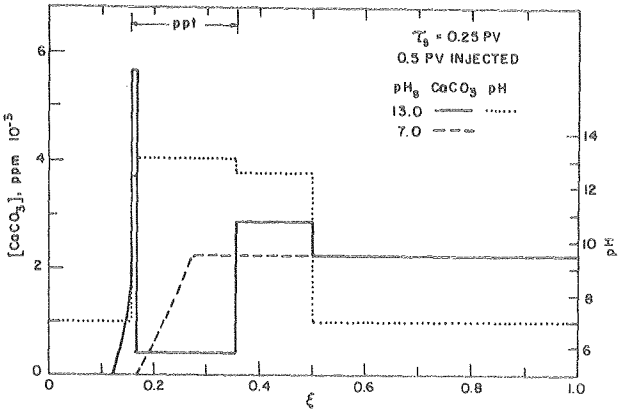

Fig. 28 - Concentration profiles after τ = 0.5 PV for a 0.25 PV pulse injection of pH 13.0 and equilibrium precipitate redissolution.

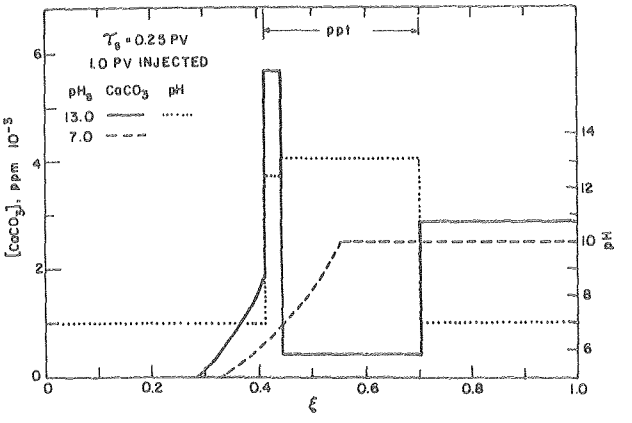

Fig. 29 - Concentration profiles after τ = 1 PV for 0.25 PV pulse injection of pH 13.0 and equilibrium precipitate redissolution.

TECHNICAL INFORMATION DEPARTMENT
LAWRENCE BERKELEY LABORATORY
UNIVERSITY OF CALIFORNIA
BERKELEY, CALIFORNIA 94720